# IMPEDANCE MATRIX COMPRESSION (IMC) USING ITERATIVELY SELECTED WAVELET BASIS FOR MFIE FORMULATIONS

**Z. Baharav and Y. Leviatan**
Department of Electrical Engineering
Technion-Israel Institute of Technology
Haifa 32000, Israel

**ABSTRACT**

*In this article we present a novel approach to incorporating wavelet expansions in method-of-moments (MoM) solutions for scattering problems described by a magnetic field integral equation (MFIE) formulation. In this approach, we utilize the fact that when the basis functions used are wavelet-type functions, only a few terms in a series expansion would be needed to represent the unknown quantity. An iterative procedure is suggested to determine these dominant expansion functions. The new approach combined with the iterative procedure yields a new algorithm that has many advantages over the presently used methods for incorporating wavelets. Numerical results that illustrate the approach are presented. © 1996 John Wiley & Sons, Inc.*
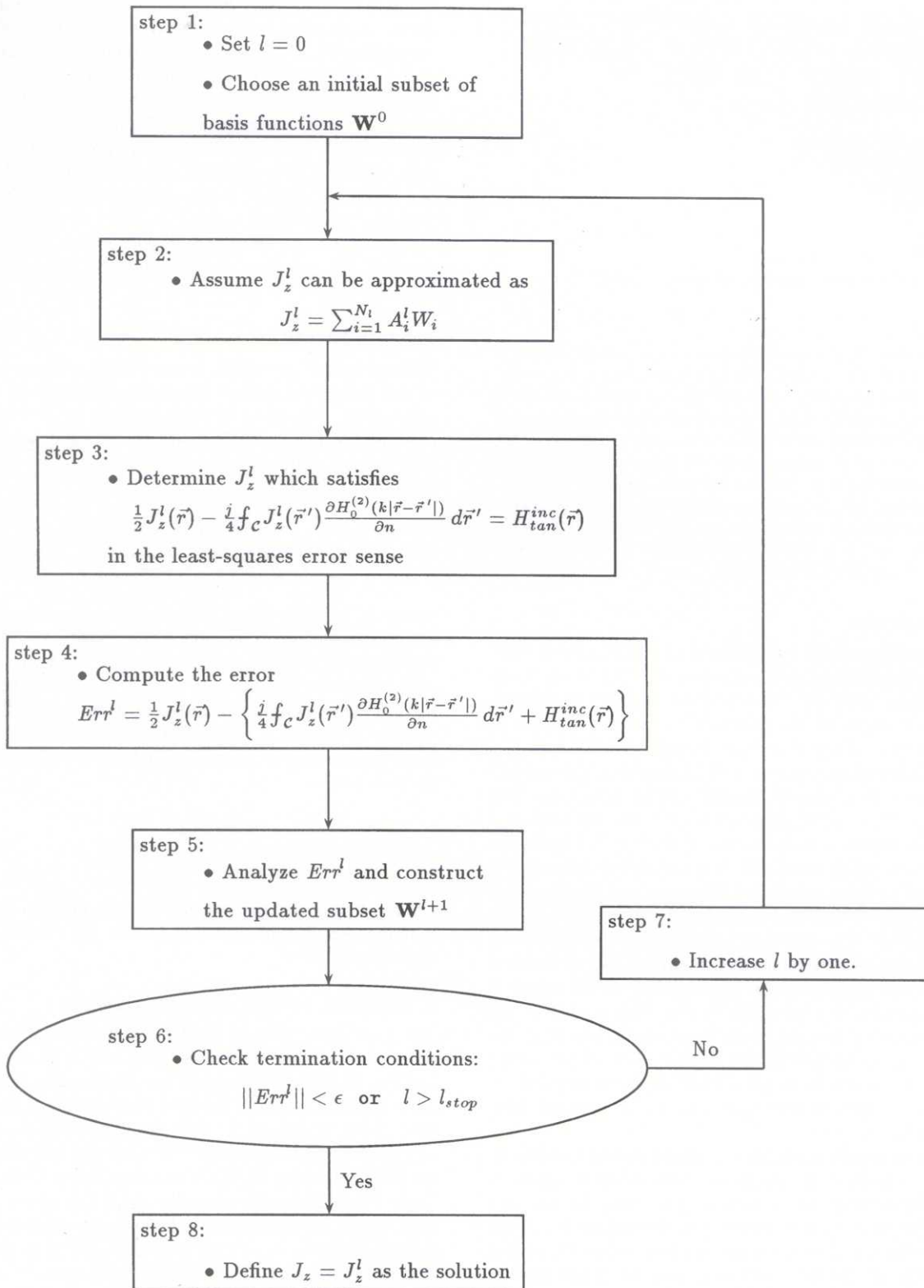
**step 1:**
- Set $l = 0$
- Choose an initial subset of basis functions $\mathbf{W}^0$

**step 2:**
- Assume $J_z^l$ can be approximated as
$$J_z^l = \sum_{i=1}^{N_l} A_i^l W_i$$

**step 3:**
- Determine $J_z^l$ which satisfies
$$\tfrac{1}{2} J_z^l(\vec{r}) - \tfrac{i}{4} \oint_C J_z^l(\vec{r}\,') \frac{\partial H_0^{(2)}(k|\vec{r}-\vec{r}\,'|)}{\partial n} \, d\vec{r}\,' = H_{tan}^{inc}(\vec{r})$$
in the least-squares error sense

**step 4:**
- Compute the error
$$Err^l = \tfrac{1}{2} J_z^l(\vec{r}) - \left\{ \tfrac{i}{4} \oint_C J_z^l(\vec{r}\,') \frac{\partial H_0^{(2)}(k|\vec{r}-\vec{r}\,'|)}{\partial n} \, d\vec{r}\,' + H_{tan}^{inc}(\vec{r}) \right\}$$

**step 5:**
- Analyze $Err^l$ and construct the updated subset $\mathbf{W}^{l+1}$

**step 6:**
- Check termination conditions:
$$||Err^l|| < \epsilon \quad \text{or} \quad l > l_{stop}$$

**step 7:**
- Increase $l$ by one.

No

Yes

**step 8:**
- Define $J_z = J_z^l$ as the solution

**Figure 1** Iterative compression algorithm. The various steps are described in more detail in the text (see Section 3)

dominant components in the wavelet domain (Step 5). In this manner, we can conjecture which are the basis functions that should be included in the expansion of the current in order to reduce the error in the immediately following iteration. These basis functions are added to the currently used set $\mathbf{W}^l$ of $N_l$ basis functions to form the updated set $\mathbf{W}^{l+1}$ comprised of

$N_{l+1}$ basis functions for the $(l+1)$th iteration. The very same process is then repeated until a desired level of accuracy is achieved (Step 6).

Note that although Steps 3–5 have been described in terms of operator equations involving continuous variables, a reduction to discretized form by means of a discretization

scheme is implicitly assumed. Thus, for example, all the integral equations are actually reduced to the appropriate matrix equations.

## 4. NUMERICAL RESULTS

In this section we consider a simple scattering problem, that of $TM_z$ plane-wave scattering by a perfectly conducting circular cylinder, as depicted in Figure 2. The incident wave is of
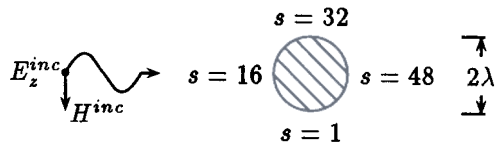
**Figure 2** Scattering problem of a circular conducting cylinder excited by a $TM_z$ incident plane wave. The length parameter along the perimeter is denoted by $s$
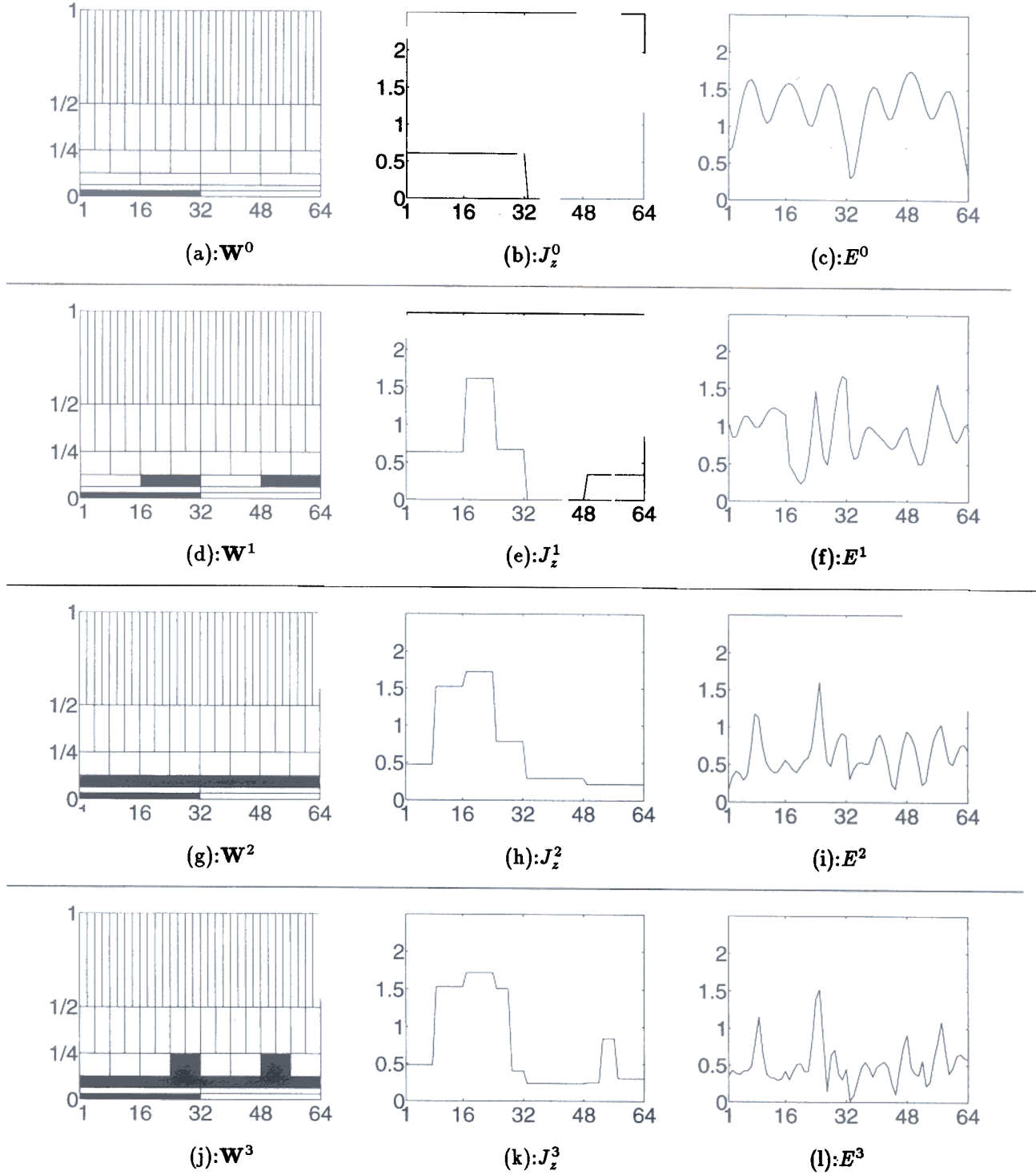
**Figure 3** Results obtained in the first four iterations of the iterative solution for the scattering problem depicted in Figure 2

unit magnetic field. The cylinder has a radius of one wavelength. The circular perimeter has been divided into 64 equally spaced pulses, which were in turn transformed into a Haar wavelet basis. The longest wavelet basis function is comprised of 32 pulses, and covers half of the cylinder circumference.

Results obtained in different iterations are depicted in Figures 3 and 4. The results obtained in each iteration are
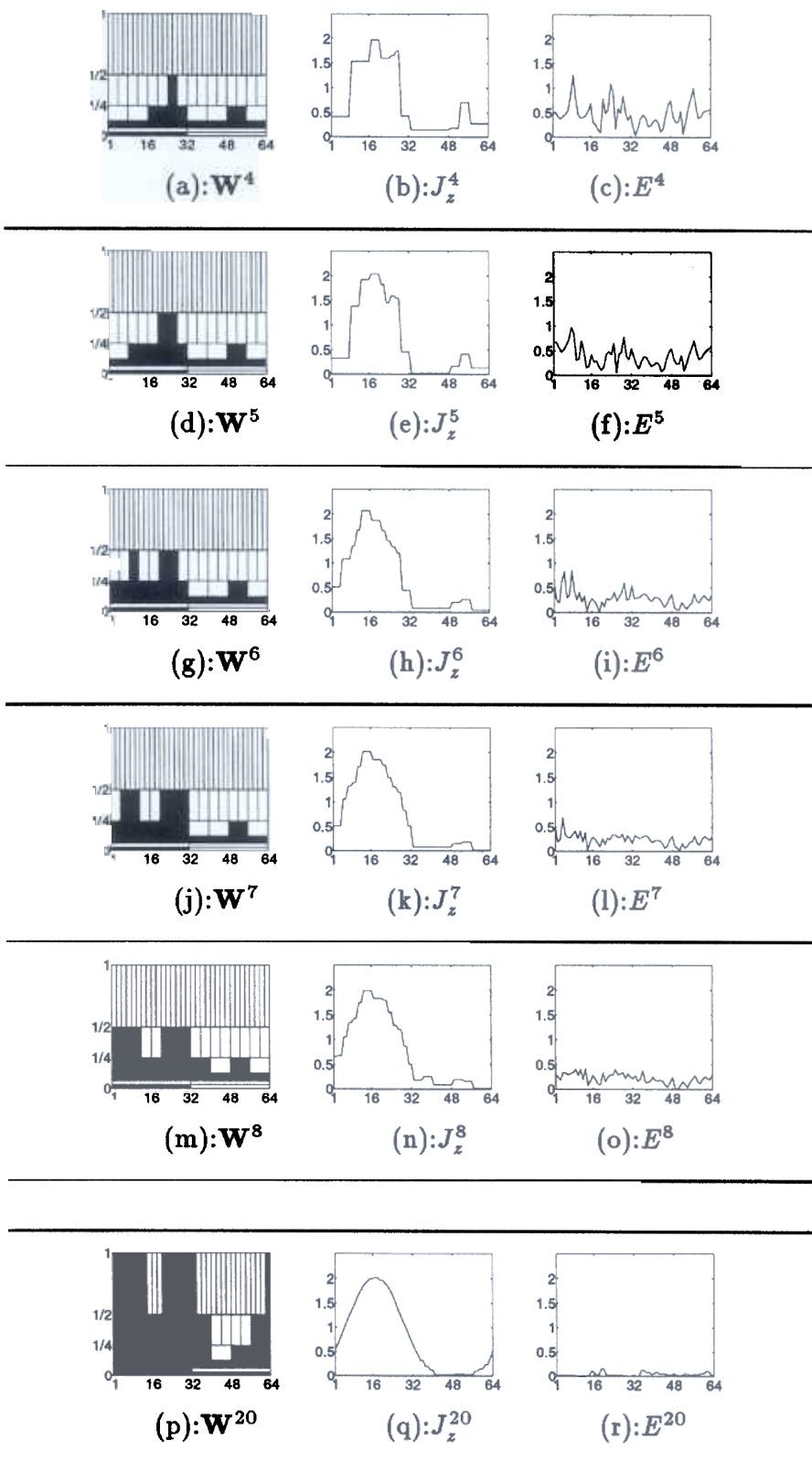


**Figure 4**  Results obtained in iterations 4–8, and iteration 20, of the iterative solution for the scattering problem depicted in Figure 2

divided into three data sets, which are represented separately in three different figures. The figures situated on the left [denoted (a), (d), (g), ... ] display the set $\mathbf{W}^l$ of wavelet basis functions on a combined-space grid. For a detailed discussion on such representations of the combined space, see, for example, [10, 11]. The horizontal axis in these figures is the spatial location, and the vertical axis describes the spatial variation. There is a total of 64 rectangles partitioning the combined space corresponding to the 64 wavelet basis functions used. The basis functions involved are denoted by black rectangles. The figures situated in the center [denoted (b), (e), (h), ... ] describe the magnitude of the approximate current density $J_z^l$ as obtained in Step 3 of each iteration. The values shown are normalized with respect to the incident magnetic field. These figures demonstrate best the progressive improvement of the approximation for the current $J_z$ achieved with this iterative scheme. The figures situated on the right [denoted (c), (f), (i), ... ] describe the error $\mathrm{Err}^l$ as evaluated in Step 4 of each iteration.

The iterative process proceeds as follows. We start with only one basis function, which is of constant amplitude over half of the cylinder (in the lit region). This basis function that constitutes the initial set $\mathbf{W}^0$ is designated by a black rectangle in Figure 3(a). Figure 3(b) shows the approximation obtained after solving for the coefficient of the basis function described in (a). The error $\mathrm{Err}^l$ is displayed in Figure 3(c). The wavelet series coefficients of this error are evaluated, and this information is analyzed to determine two additional basis functions, which together with the initial set $\mathbf{W}^0$ form the updated set $\mathbf{W}^1$ shown in Figure 3(d). A similar explanation can be given to the rest of the figures. Figure 3 describes the first four iterations, and a few more iterations are described in Figure 4. The last iteration shown is the 20th iteration, which involves 41 basis functions. A reference solution is depicted for comparison in Figure 5. The reference solution is the one that involves all the 64 basis functions.

Finally, we compare the new approach suggested herein and the conventional one, where the impedance matrix undergoes thresholding, which enables the solution of the matrix equation by a sparse matrix solver. Extensive comparison between the thresholding method and the impedance matrix compression method can be found in [8]. The scattering problem considered is that depicted in Figure 2, except that the cylinder radius is now assumed to be $2\lambda$ long, and 128 basis functions are used for discretization. Figure 6 describes the performance of the two algorithms, demonstrating the advantage of the new algorithm. The vertical axis describes the $L_2$ norm of the error in satisfying the boundary condi-

tion. The horizontal axis is the compression ratio. The compression ratio is equal to 1 minus the ratio between the number of nonzero elements of $[\mathscr{Z}^l]$ in the last iteration preformed and the number of elements of the original matrix. Note that although we consider the matrix $[\mathscr{Z}^l]$ in the last iteration as a measure of complexity, one must recall that other matrix equations, albeit smaller in size, have been solved in the preceding iterations. It should be added that in order to take full advantage of the IMC approach, the matrix $[\mathscr{Z}^l]$ is also subjected to a thresholding operation. In the thresholding operation, the smallest (in magnitude) elements of $[\mathscr{Z}^l]$ are replaced by zeros, and this procedure continues as long as the error level does not exceed by 30% the error level that would have been obtained had $[\mathscr{Z}^l]$ not undergone thresholding. Another perspective on the difference between the methods can be gained from Figure 7. The approximate current obtained based on the thresholding procedure is shown in Figure 7(a), whereas the one obtained based on the new algorithm is shown in Figure 7(b). The fields due to these currents satisfy the boundary condition to within the same prescribed error level of 1%. It is seen that the current shown in Figure 7(a) has many rapidly varying ripples. The wiggly behavior of the solution stems from the fact that all the rapidly varying wavelets are actually playing a part in the solution. In contrast, only part of these wavelets are used to construct the solution shown in Figure 7(b), and hence this solution is smoother.

## 5. SUMMARY AND CONCLUSIONS

In this article a new algorithm for the incorporation of wavelets into the solution of integral equations arising in scattering problems has been proposed. This algorithm rests on the fact that quite often only a few terms are needed to describe the current on the scatterer to a good approximation. An iterative procedure for the determination of these few terms has been presented. The procedure is based on the apparent correlation between the respective wavelet expansions of the above-defined error and the unknown current.
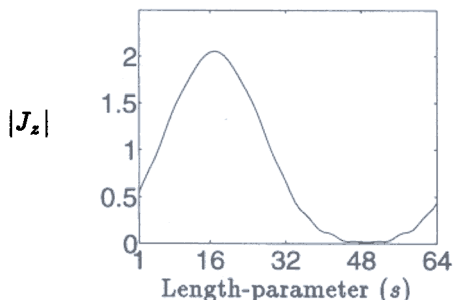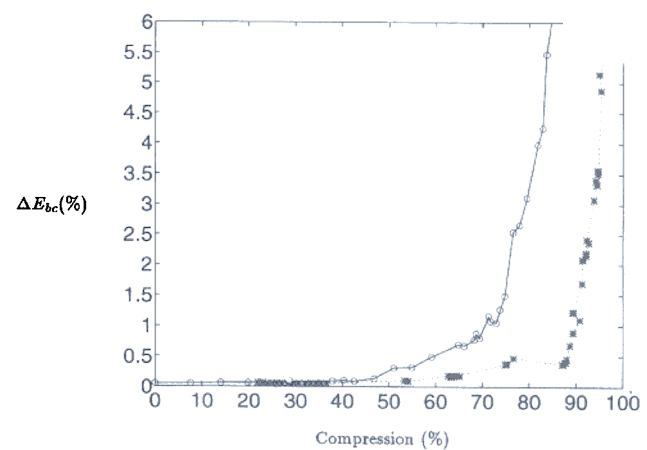
**Figure 6** Boundary-condition error versus compression of the impedance matrix for a scattering problem similar to that illustrated in Figure 2, obtained by two solution methods. In this case, the radius is $2\lambda$, and the number of elements taken is 128. Cases considered are for the conventional approach of thresholding the original impedance matrix based on wavelets (denoted by circles and the solid line), and for the iterative compression algorithm proposed in this article (denoted by stars with the dotted line)
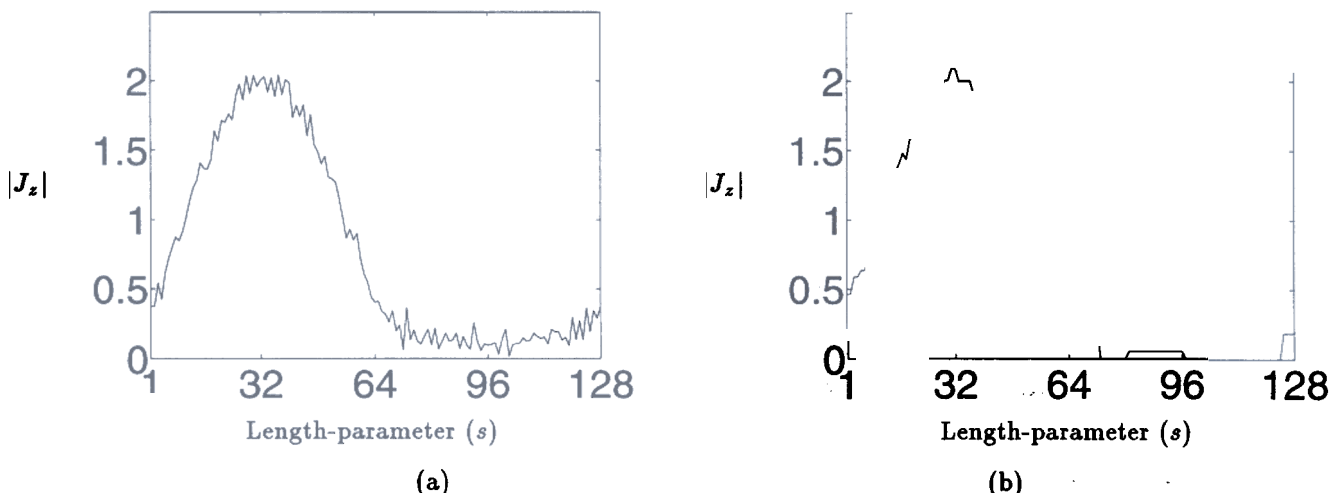
**Figure 5** Magnitude of current density $J_z$ along the circular perimeter of the scatterer, for the scattering problem illustrated in Figure 2, obtained with 64 basis functions

**Figure 7** Magnitude of current density $J_z$ along the perimeter of the cylinder obtained by two solution methods: Cases considered are for (a) the conventional method of thresholding the impedance matrix, and (b) the iterative compression algorithm proposed in this article (after 26 iterations). Both solutions are subject to the same accuracy requirements in terms of satisfying the boundary condition

Numerical results have been given to demonstrate the applicability and features of the algorithm.

## REFERENCES

1. B. Z. Steinberg and Y. Leviatan, "On the Use of Wavelet Expansions in the Method of Moments," *IEEE Trans. Antennas Propagat.*, Vol. 41, no. 5, 1993, pp. 610–619.
2. H. Kim and H. Ling, "On the Application of Fast Wavelet Transform to the Integral-Equation Solution of Electromagnetic Scattering Problems," *Microwave Opt. Technol. Lett.*, Vol. 6, No. 3, 1993, pp. 168–173.
3. R. L. Wagner, G. P. Otto, and W. C. Chew, "Fast Waveguide Mode Computation Using Wavelet-Like Basis Functions," *IEEE Microwave Guided Wave Lett.*, Vol. MGW-3, No. 7, 1993, pp. 208–210.
4. B. Z. Steinberg and Y. Leviatan, "Periodic Wavelet Expansions for Analysis of Scattering from Metallic Cylinders," *Microwave Opt. Technol. Lett.*, Vol. 7, No. 6, April 1994, pp. 266–268.
5. J. C. Goswami, A. K. Chan, and C. K. Chui, "An Analysis of Two-Dimensional Scattering by Metallic Cylinders Using Wavelets on a Bounded Interval," *IEEE AP-S Int. Symp. Dig.*, Vol. 1, 1994, p. 2.
6. R. R. Coifman and M. V. Wickerhauser, "Entropy-Based Algorithms for Best Basis Selection," *IEEE Trans. Inform. Theory*, Vol. IT-38, No. 2, 1992, pp. 713–718.
7. Chee-Hung Henry Chu, "Data Compression by Multiresolution Tree Search," *Opt. Eng.*, Vol. 33, No. 7, 1994, pp. 2136–2142.
8. Z. Baharav and Y. Leviatan, "Impedance Matrix Compression Using Wavelet Expansions," *IEEE Trans. Antennas Propagat.*, to be published.
9. N. Morita, N. Kumagai, and J. R. Mautz, *Integral Equation Methods for Electromagnetics*, Artech House, Boston, 1990.
10. C. Herely et al., "Tilings of the Time-Frequency Plane: Construction of Arbitrary Orthogonal Bases and Fast Tiling Algorithms," *IEEE Trans. Signal Proc.*, Vol. SP-41, No. 12, 1993, pp. 3341–3359.
11. I. Daubechies, *Ten Lectures on Wavelets*, Society for Industrial and Applied Math., Philadelphia, 1992.

# COMPACT ANECHOIC CHAMBER AND ANTENNA MEASUREMENT SYSTEM FOR MICROWAVE TEACHING AND RESEARCH APPLICATIONS

**D. Geen and D. Smith**
Department of Electrical, Electronic Engineering and Physics
University of Northumbria at Newcastle
Newcastle-upon-Tyne, NE1 8ST, England

**ABSTRACT**
*The design of a small, low-cost anechoic chamber well suited to the teaching of antenna theory and measurement techniques is described. The chamber design allows for dismantling, relocation, and reassembly when required. Its performance in the range 18–30 GHz has been found to be good. The incorporation of the chamber into an automated antenna pattern measurement system for education and research purposes is also described. © 1996 John Wiley & Sons, Inc.*

## INTRODUCTION

The teaching of antenna theory can be greatly assisted by the use of practical demonstrations to illustrate various antenna characteristics, such as beamwidth and side-lobe performance for different antenna orientations. In an academic environment such measurements can be difficult to perform because of the uncertain nature of reflections from objects in the vicinity of the test area and also the general difficulty in setting up and aligning the required apparatus.

Traditionally, antenna testing has been performed on open ranges or in shielded anechoic rooms permanently designed for such purposes and established at considerable cost. For the present application it was decided to investigate the possibility of constructing a low-cost anechoic chamber that could be regarded more as a transportable piece of test equipment than a fixed structure. Such an item could be used in a number of teaching and research laboratories alongside existing equipment.